Article

Journal of
Nanoscience and Nanotechnology
Vol. 17, 1321–1328, 2017
www.aspbs.com/jnn

Chitin and Chitosan Based Hybrid Nanocomposites for Super Capacitor Applications

S. Anandhavelu[1], V. Dhanasekaran[2,*], V. Sethuraman[3], and Hui Joon Park[2]

[1] Department of Chemistry, VelTech-MultiTech-Dr.Rangarajan-Dr.Sakunthala Engineering College, Chennai 600062, Tamilnadu, India
[2] Division of Energy Systems Research, Ajou University, Suwon 443-749, Republic of Korea
[3] Department of Industrial Chemistry, School of Chemical Sciences, Alagappa University, Karaikudi 630003, Tamilnadu, India

In this paper, we report a facile low-cost synthesis of the chitin and chitosan-based hybrid nanocomposites for supercapacitors. The chitosan and chitin based hybrid composites functional group analysis, structural, optical and morphological properties were characterized using FTIR spectroscopy, Raman spectroscopy, UV-vis spectroscopy and scanning electron microscopy (SEM), respectively. Specific capacitance values of hybrid composites were calculated using cyclic voltammetry, electrochemical impedance spectroscopy and galvanostatic charge–discharge analysis. The hybrid composites asymmetric supercapacitor performance was perceived in the range of −0.2 to 1.0 V. The specific capacitance value was achieved at 542.63 F g^{-1} at current density value of 0.1 A g^{-1} for CH-GO-ZnO/PANI hybrid composites. The prepared hybrid nanocomposites exhibit good supercapacitive performance and long-term cycle stability. These results demonstrate the potential of the CH-GO-ZnO/PANI hybrid nanocomposites as a high-performance supercapacitors.

Keywords: Electrochemical Deposition, Nano Composite, Chitosan, Chitin, Supercapacitor.

1. INTRODUCTION

Supercapacitors, a novel kind of energy storage device, also known as electrochemical capacitors, has received much attention to use in hybrid electric vehicles, memory backup, transportable systems, mobile equipment, and small energy grids due to their higher power density, superior cycle lifetime and low maintenance cost. In recent research in supercapacitors has been carried out for high energy storage and flexibility with an importance on the progression of novel electrode materials.[1–3] During the past few years, carbon materials, mixed metal oxide and conducting polymers have been extensively studied in supercapacitors.[4–7] Transition metal oxides and conducting polymers are the promising candidates because they can provide high energy density for pseudocapacitors. It has been found that carbon materials which combine with pseudocapacitive electrode materials can improve the capacitance of supercapacitors.[8–10] Graphene is an atom-thick, two-dimensional (2D) material composed of a monolayer hexagonal sp^2-hybridized carbon, which has maximum surface area of 2,630 m^2 g^{-1} and high intrinsic electrical conductivity and is believed to be one of the most promising electrode materials for supercapacitors.[11–14] However, in practical applications, graphene usually suffer from agglomeration or restacking due to strong van der Waals interactions,[15–17] which overcome by metal/metal oxide or metal hydroxide nanoparticles.[18–21] It is well known that metal oxides such as RuO_2, MnO_2, IrO_2 and NiO_x can be improve their capacitance of carbon-based supercapacitors and it can be contribute as a pseudo-capacitance to the total capacitance apart from the double-layer capacitance of carbon materials.[22–24] However, their expensive nature, low abundance and high toxicity severely limit their practical application in a large scale.[22,24,25] Therefore, the development of low-cost and high-abundance metal oxide as an alternative is highly desirable for future purposes.[26–29] ZnO is considered to be a promising material for supercapacitors due to its high specific energy density of 650 A/g, low cost, non-toxicity, eco-friendliness, good electrochemical activity and abundant availability.

*Author to whom correspondence should be addressed.

Recently, Chen et al.,[30] reported that graphene oxide–MnO nanocomposites for supercapacitors and their specific capacitance value was 197.2 F/g. A reduced graphene oxide was pasted on the ITO glass substrate followed by depositing ZnO nanoparticles by ultrasonic spray pyrolysis for supercapacitors by Zhang et al.[31] In their work, specific capacitance of their supercapacitor was 61.7 F/g, which was larger than that of bare rGO electrode. A sandwiched nanoarchitecture of reduced graphene oxide/ZnO/deducted graphene oxide was fabricated by GuO et al.[32] using chemical vapor deposition method, which exhibited a specific capacitance of 51.6 F g^{-1} at a scan rate of 10 mV s^{-1}. The graphene-ZnO exhibited a high specific capacitance of 156 F g^{-1} at a scan rate of 5 $mV \cdot s^{-1}$ and it exhibits good supercapacitive performance and long-term cycle stability.[33] Furthermore, graphene-ZnO nanocomposites synthesized by ultrasonic spray pyrolysis method and their electrochemical performance were reported.[31,34] However, these materials were limited by a low specific capacitance and poor stability at higher scan rate or high current densities. An effective regulation of graphene-ZnO hybrid for high performance of supercapacitors is still challenging.

High electrical conductivity of materials is one of the most critical requirements for myriad of applications including energy-related devices and conducting polymers. High surface carbon materials or noble metal oxides and conducting polymer composites are being extensively studied today.[35] However, the poor conductivity and weak flexibility of some conducting polymers often limit them usage in high-performance devices.[36] There is continued interest in polyaniline (PA)-based materials because of their cost effectiveness and way of synthesis.[37] Furthermore, PA is an excellent organic conductor with good environmental stability and biocompatibility,[38] and it has used to fabricate composites with carbonaceous materials for supercapacitor electrodes[39] and sensors. The advantages of carbon materials are combined with PA, the resulting composites provided synergistic performance as electrode materials.[40,41] The study on the intercalation of PANI and its derivatives into graphite oxide is reported recently.[42,43]

In recent times, the growth of chitosan based novel nanocomposites is attracting many researchers due to their higher specific capacitance and good cyclic capacity for supercapacitor applications.[44] Chitosan is one of the second abundant natural biopolymers on the earth. It has been extensively investigated for several decades for biosensors, separation membrane, artificial skin, bone substitutes, water treatment, and so on, because of its biocompatibility, biodegradability, multiple functional groups, as well as its solubility in aqueous medium.[45] However, numerous advantages and unique properties of chitosan but the mechanical properties of chitosan could not satisfy the required level of applications. The formation of organic–inorganic hybrids through incorporation of fillers is an effective approach for improving physical and mechanical properties of chitosan. We reported earlier the preparation of chitosan-ZnO nanostructures[46] with controlled addition of sodium hydroxide into zinc chloride and chitin solution.

In this report, a simple and facile synthesis route is developed to prepare chitosan and chitin based graphene oxide-ZnO/PANI hybrid as an electrode material for supercapacitors using chemical synthesis. Initially, graphene oxide (GO) was synthesized using the well-known modified Hummers and Offeman procedure. Polymerization was carried out using PA monomer, GO, zinc chloride and chitosan samples. This strategy provides a feasible method for the preparation of highly active hybrid materials, which show high specific capacitance and excellent cycle stability for supercapacitors. Such high electrochemical properties provide important prospects for chitosan and chitin based graphene oxide-ZnO/PANI hybrid to be widely used as electrode material in supercapacitor.

2. EXPERIMENTAL DETAILS

2.1. Materials

The high quality commercially available graphite powder was used in this preparation method. The aniline (ANI), sulfuric acid, potassium permanganate, hydrogen peroxide, zinc chloride, ammonium persulfate, hydrochloric acid, acetic acid, N-methyl-2-pyrrolidone (NMP) and sodium hydroxide were used in this preparation process. The 90% deacetylated chitosan sample was purchased for preparation process. To prepare chitin, the shells of crab were scraped free of loose tissue, washed, dried and ground to pass through a 250 μm sieve and then subjected to a demineralization using 4% hydrochloric acid and deproteinization with 4% sodium hydroxide solution for 2 h separately.

2.2. Preparation of GO

Graphene oxide was synthesized from powdered flake graphite (12,500 meshes) by a modified Hummers and Offeman procedure.[47] An approximately 3 g of graphite powder was mixed into 12 mL of concentrated H_2SO_4 and then the sample was subjected to heating process at 80 °C for 5 h. The collected sample was inclusion in sonication process at 30 °C and then solution was filtered using a 200 nm porous filter to retrieve the pre-oxidized graphite powder. To exfoliate the pre-oxidized graphite powder into monolayer graphene sheets, the 2 g of pre-oxidized graphite powder and 15 g of $KMnO_4$ were added into 120 ml of H_2SO_4 solution and stirred for 2 hours, keeping the beaker in an ice-water bath to ensure the temperature remained below 10 °C. Hereafter, 120 mL of H_2O_2 (30 wt% aqueous solution) was added to the above liquid, and the mixture was stirred up to 2 h in 30 °C. Finally, the resulting suspension was filtered and washed with 10% HCl—deionized water. The obtained GO was dispersed in deionized water to form a stable brown solution.

2.3. Preparation of Hybrid Composites

The 1 M HCl aqueous solution dissolved 0.25 g chitin and 1 M HCl aqueous solution dissolved 0.5% aniline monomer were mixed. The 20 ml of synthesized GO solution was added with stirring process and then 5% of zinc chloride solution was incorporated with 10 min interval to this solution. The 10 mL of 0.1 g of oxidant ammonium persulfate dissolved 1 M HCl solution was added with 10 minutes interval and then micro addition of 50 mL of 0.2 M NaOH aqueous solutions. Polymerization was carried out until the characteristic green color of polyaniline emeraldine salt appeared. The mixture was included in vigorous stirring up to 30 min. Finally the sample was diluted using 100 mL of water. The precipitated polymer was collected by filtration process and washed using de-ionized water, thereafter dried in hot air oven at 60 °C. The prepared sample was designated as CH-GO-ZnO/PANI. The similar procedure was used to prepare CS-GO-ZnO/PANI sample by using with chitosan instead of chitin. In addition to that, CS-GO/PANI sample was prepared without addition of zinc chloride solution and CS/PANI sample was prepared without addition of zinc chloride and GO solution in the above preparation process.

2.4. Preparation of Electrodes

A mixture of 80 wt% of the materials, 10 wt% of acetylene black and 10 wt% of polyvinylidene difluoride (PVdF) as a binder with a weight ratio of 80:10:10 were sufficiently mixed in 3 ml of N-methyl-2-pyrrolidone (NMP) solvent as a paste. This paste was coated onto the stainless steel (1 cm^2) electrode and dried in an oven at 110 °C for overnight before the electrochemical test. This served as the working electrode. Three electrode cell systems were used to evaluate the electrochemical performance by electrochemical impedance spectroscopy (EIS), cyclic voltammetry (CV) and galvanostatic charge–discharge techniques (Autolab-BSTR 10A) at room temperature. The electrolyte was used as a 0.2 M H_2SO_4 aqueous solution. A platinum and saturated calomel electrode (SCE) was used as a counter and reference electrodes, respectively.

2.5. Materials Characterization

The function group analysis was studied using FTIR spectroscopy (Thermo-Nicolet-380 Madison, USA) in the range of 4000–400 cm^{-1} at room temperature. Surface morphological properties of composites were analyzed using HR-SEM (FEI Quanta FEG 200-High Resolution Scanning Electron Microscope). The absorption spectra were recorded using UV–vis spectrophotometer (2401 PC model; Shimadzu, Kyoto, Japan) in the wavelength range of 200–800 nm. Raman scattering analysis was performed to investigate functional group confirmation by HORIBA Jobin Yvon, LabRAM HR-800 micro Raman spectrometer. The specific capacitances performances were analyzed by electrochemical impedance spectroscopy (EIS), cyclic voltammetry (CV) and galvanostatic charge–discharge techniques (Autolab-BSTR 10A).

3. RESULTS AND DISCUSSION

The characteristic peaks of PANI, chitosan and GO are observed in FTIR spectra of CS/PANI, CS-GO/PANI, CS-GO-ZnO/PANI and CH-GO-ZnO/PANI composites as shown in Figure 1. An infrared peak is observed at 3323 cm^{-1} corresponds to N–H stretching which may be due to the hydrogen bonded with 20 amino groups and O–H stretching vibration. The absorption peak is observed at 1649 cm^{-1} due to the C═O stretching carbonyl group of graphene oxide. In addition to that, C═C stretching of quinoid rings of PA and N–H stretching vibration of primary amine, C═C stretching vibration of benzenoid rings, C–N stretching related peaks are observed at 1514 cm^{-1}, 1462 cm^{-1} and 1284 cm^{-1}, respectively. The absorption peak is observed at 1112 cm^{-1} wave number due to N = Q = N bending vibration and it has shifted to be lower wave number for PA. The peak is observed at 1130 cm^{-1} which is attributed to the hydrogen bonding between chitosan and amine group of the grafted chain of PANI. The absorption band at 830 and 750 cm^{-1} is assigned to aromatic C–H bending vibration and chitosan characteristic peaks of muco-polysaccharide, respectively. The characteristic peak of Zn–O stretching vibration is emerged at 426 cm^{-1} (Figs. 1(c and d)) for CS-GO-ZnO/PANI and CH-GO-ZnO/PANI hybrid composites.[48,49] There are large amount of oxygenous groups in the graphene oxide sheets, which can easily interact with the nitrogen atoms in the –NH– group of chitosan and PANI backbone through –O–H···N– and –O···H–N– hydrogen bonds. FTIR spectral studies suggest the copolymerization of PA, chitosan and ZnO on to GO sheets.

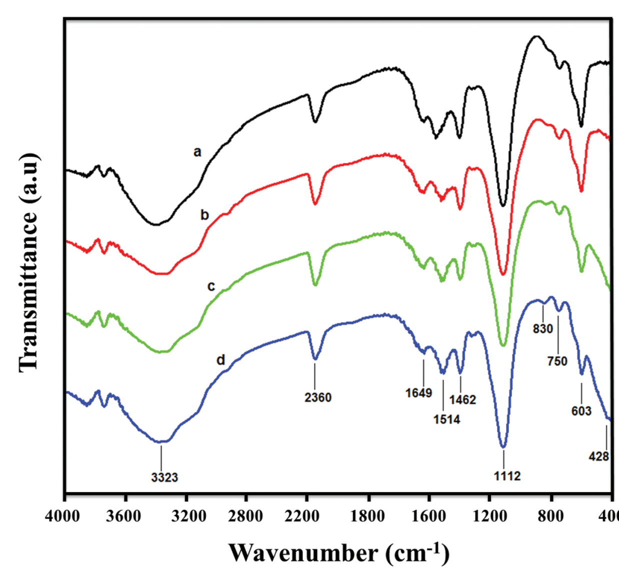

Figure 1. FTIR spectra of hybrid composites (a) CS/PANI, (b) CS-GO/PANI, (c) CS-GO-ZnO/PANI and (d) CH-GO-ZnO/PANI.

Raman spectroscopy is used to study pictorial representation of the chemical bonding structure.[50] The Raman scattering spectra are observed for hybrid composites of CS/PANI, CS-GO/PANI, CS-GO-ZnO/PANI and CH-GO-ZnO/PANI as shown in Figure 2. The broad peak is observed at 1552 and 3233 cm^{-1} for composites of CS/PANI, CS-GO/PANI and CS-GO-ZnO/PANI as shown in Figures 2(a–c), which is corresponds to PANI and it has reported by Kurita et al.[51] The broad D mode peak is spited in to two peaks in CH-GO-ZnO/PANI hybrid composite and it has observed in Raman shift 1343, 1602 cm^{-1} as shown in Figure 2(d). The higher wavenumber observed Raman shift has disappeared in CH-GO-ZnO/PANI hybrid composite. The significant structural changes have occurred during the chemical processing from natural graphite to GO and the formation of CH-GO-ZnO/PANI which is obviously reflected in the Raman scattering. The Raman scattering of the natural graphite showed that the prominent G peak at 1590 cm^{-1}, corresponding to the first-order scattering of the E_2g mode. On the other hand, the spectrum of the as-prepared GO displayed two prominent peaks at 1350 and 1590 cm^{-1}, which corresponded to the well-documented D mode or the phonon mode of a sp^2-hybridized carbon to a sp^3-hybridized carbon and the G mode vibration of a sp^2-hybridized carbon, respectively.[52]

Figure 3 shows the UV-Vis absorption spectra of CS/PANI, CS-GO/PANI, CS-GO-ZnO/PANI and CH-GO-ZnO/PANI. The PANI characteristic peaks are observed in the range of 283–308 nm and it has shifted to the lower value of the samples (Fig. 3(a)). The absorption peak is observed at 233 and 300 nm, which can be assigned to the $\pi \rightarrow \pi^*$ transitions of aromatic C–C bonds and $n \rightarrow \pi^*$ transitions of C–O bonds, respectively for synthesized

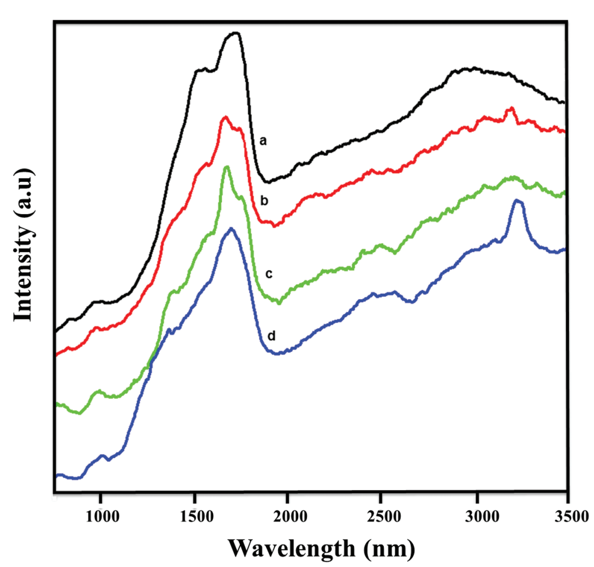

Figure 2. Raman spectra of hybrid composites (a) CS/PANI, (b) CS-GO/PANI, (c) CS-GO-ZnO/PANI and (d) CH-GO-ZnO/PANI.

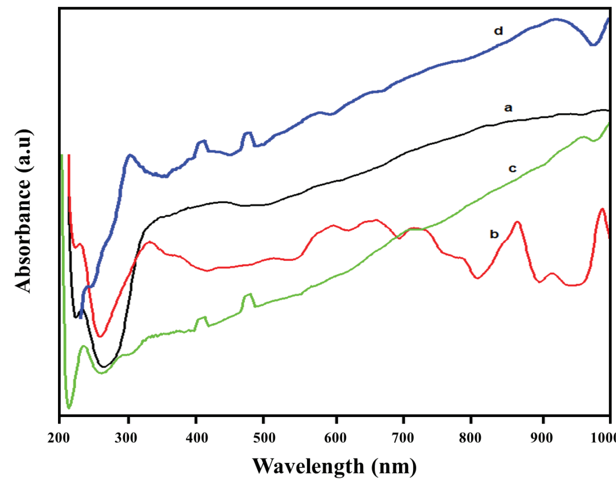

Figure 3. UV-VIS spectra of hybrid composites (a) CS/PANI, (b) CS-GO/PANI, (c) CS-GO-ZnO/PANI and (d) CH-GO-ZnO/PANI.

RGO in Figures 3(b–d). The absorbance maximum is exhibited at 283–308 nm corresponds to the $\pi \rightarrow \pi^*$ (λ1) transition for benzenoid segment.[53] The wavelength of the quinoid band plays an important role for switching the polyaniline from an electric insulator to a doping conductor. Furthermore, the intensity ratio of AQ/AB indicated the relative amount of quinoid unit in polyaniline. ZnO showed an absorption (broad) peak at 365 nm for CS-GO-ZnO/PANI and CH-GO-ZnO/PANI samples (Figs. 3(c and d)), respectively. The absorption peak of GO is exhibited at 233 nm and shifted to 201 nm for CH-GO-ZnO/PANI. The blue-shift is attributed to strong coupling effect between graphene sheets and the semiconductor nanoparticles.[54–57]

The typical micrographs of CS/PA, CS-GO/PANI, CS-GO-ZnO/PANI and CH-GO-ZnO/PANI hybrid composites are observed by HRSEM as shown Figure 4. The CS/PANI composite (Fig. 4(a)) micrograph revealed that the sheet-like grains for PANI and CS matrix without any agglomeration and it may be due to the binding between PANI and CS.[58] The grains size was exhibited in the range of 2.30–2.59 μm. The fibrillar morphology has observed for 20 mL of synthesized GO mixed with CS/PANI composite as shown in Figure 4(b). This formation may be due to the electrostatic attraction of between the CS, GO and PANI of CS-GO/PANI composites. The formation of ZnO using zinc chloride and sodium hydroxide solution in the CH-GO-ZnO/PANI and CS-GO-ZnO/PANI hybrid composites is enhanced the bond formation between CS, GO and PANI in Figures 4(c and d). The finite flower like grains are seen in the CH-GO-ZnO/PANI hybrid composite, while sheet-like grains are observed on the CS-GO-ZnO/PANI hybrid composite. It is well known that, graphene oxide is an acceptor and chitosan and aniline is an electron donor. When HCl is used as a dopant, the chitosan and aniline monomer absorbed on surface of GO through the electrostatic attraction resulting

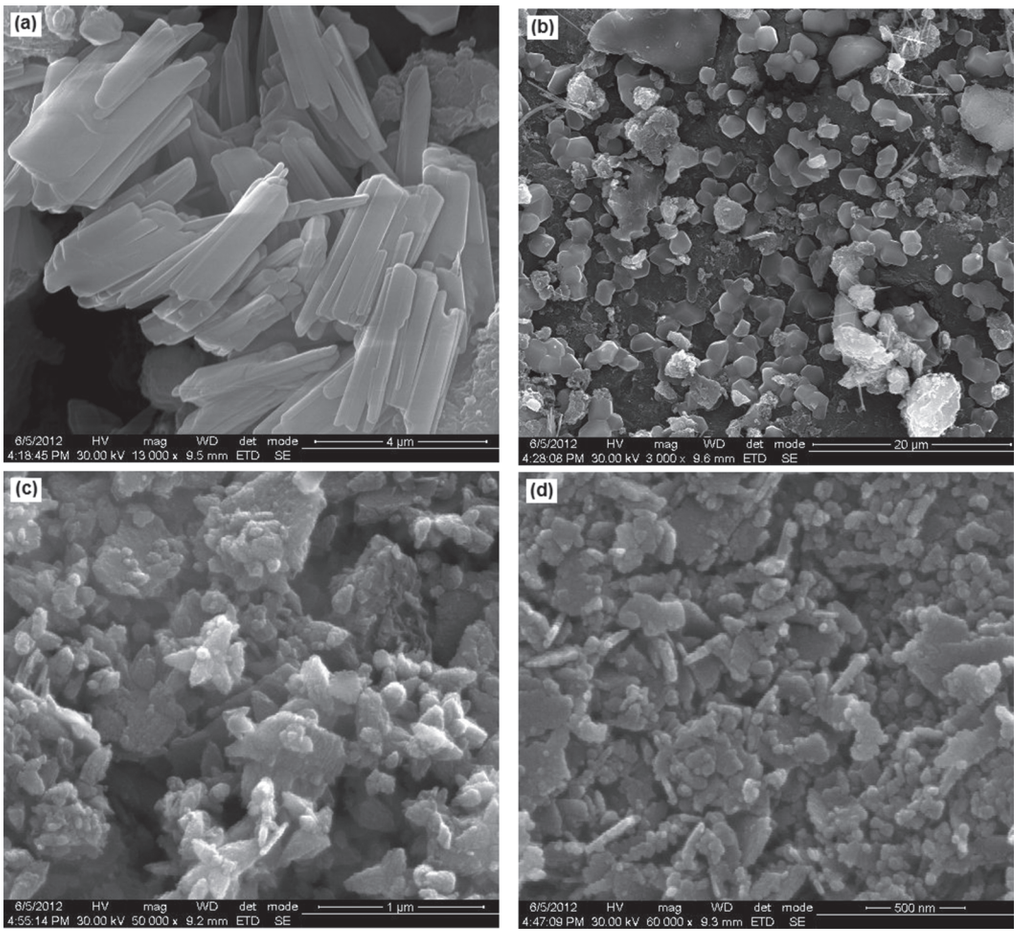

Figure 4. Typical HRSEM images of hybrid composites (a) CS/PANI, (b) CS-GO/PANI, (c) CS-GO-ZnO/PANI and (d) CH-GO-ZnO/PANI.

a formation of weak charge-transfer complexes between the chitosan, aniline monomer and GO. As a result of this absorption process, GO sheets are finely coated by PANI particles by *in-situ* preparation of GO from the polymerization aniline monomer. The absorption behavior of aniline monomer on the whole surface of graphene oxide is caused a continuous PANI coating on the GO sheets. The graphene oxide nanosheets can be considered as a supporting material of PANI growth to provide a large number of active nucleation sites.

The electrode materials for supercapacitor application are evaluated by standard cyclic voltammetry (CV) and galvanostatic charge–discharge technique. Figure 5 is represented that the CV curves of CS/PANI, CS-GO/PANI, CS-GO-ZnO/PANI and CH-GO-ZnO/PANI composites using 0.2 M H_2SO_4 as an electrolyte, potential range −0.2 to 1.0 V versus SCE and 100 mVs^{-1} scan rate. In the case of CS/PANI composite, there is a couple of redox peaks observed in CV curve, due to the redox transition of PANI between the semiconducting state (leucoemeraldine form) and conducting state (polaronic emeraldine form),[59, 60] leading to the redox capacitance. The supercapacitor based on CH-GO-ZnO/PANI composite is exhibited an approximately rectangular shape, implying that its capacitance value is mainly attributed to electric double layer capacitance. The CV curves area of CH-GO-ZnO/PANI and CS/PANI composites is apparently larger than that of CS-GO/PANI and CS-GO-ZnO/PANI, may be due to the higher specific capacitance. CH-GO-ZnO/PANI in the composite is offered highly conductive path and served as a high surface area backbone for the polymerization of PANI, facilitating rapid transport of the electrolyte ions into the electrode during rapid charge/discharge process.[61] Quasi-rectangle area of CH-GO-ZnO/PANI CV curve is larger than CS-GO-ZnO/PANI and it has suggested that the larger capacitance properties.

Electrochemical impedance spectroscopy (EIS) is a complementary technique galvanostatic cycling measurements which provides more information about the electrochemical frequency behavior of the system. Impedance measurements can also study the redox reaction resistance and equivalent series resistance. Impedance measurements are performed for CS/PANI, CS-GO/PANI, CS-GO-ZnO/PANI and CH-GO-ZnO/PANI composites

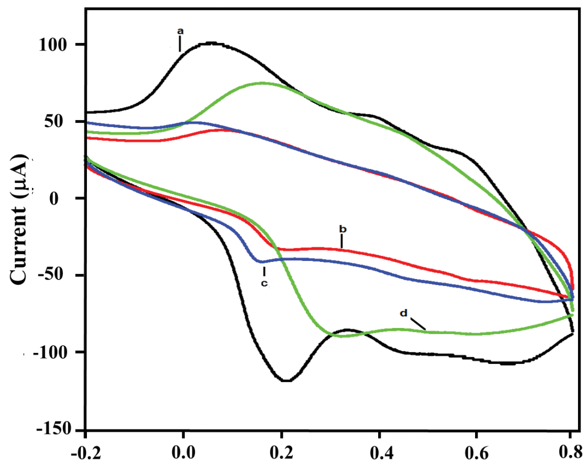

Figure 5. Cyclic voltammogram of hybrid composites such as (a) CS/PANI, (b) CS-GO/PANI, (c) CS-GO-ZnO/PANI and (d) CH-GO-ZnO/PANI. In this measurement was carried out in 0.2 M H_2SO_4 electrolyte solution using hybrid composites deposited stainless steel as a working electrode, Pt foil as a counter electrode and saturated calomel electrode (SCE) as a reference electrode with the scan rate 100 mV/s.

using in 0.2 M H_2SO_4 aqueous electrolyte by EIS. EIS are collected with a frequency range of 0.1 Hz–10 kHz and a DC bias of 10 V. The EIS data are analyzed using Nyquist plots and it show the frequency response of the electrode/ electrolyte system with a plot of the imaginary component (Z'') of the impedance against the real component (Z'). Each data point is at a different frequency with the lower left portion of the curve corresponding to the higher frequencies. The vertical curve corresponds to a cell more closing to an ideal capacitor. As shown in Figure 6, the equivalent series resistance (ESR) of the electrode can be obtained from the x intercept of the Nyquist plot. All the materials showed comparable ESR at about 1.8 Ω. The Nyquist plots of CS/PA, CS-GO/PANI, CS-GO-ZnO/PANI and CH-GO-ZnO/PANI exhibited semicircles over the high frequency range, followed by a straight line in the low frequency region in Figures 6(a–d). Large semicircles observed for these electrodes are indicative of high interfacial charge-transfer resistance. The semicircle at high frequency is not detected for CS-GO/PANI in Figure 6(e) (Inset of lower scale value), suggesting that interfacial charge-transfer resistance among CS-GO/PANI has significantly low because of the high conductivity. CS-GO-ZnO/PANI and CH-GO-ZnO/PANI has some interfacial charge-transfer resistance than the composites CS/PANI and CS-GO/PANI. The slight enhancement of interfacial resistance could be attributed to the inclusion of semiconducting behaviour ZnO. Except for the low electrical resistance, CH-GO-ZnO/PANI exhibited as short and equal diffusion path length of the ions in the electrolyte, as seen from the Warburg region on the Nyquist plots. Ions of the electrolyte did not penetrate into the particulate and accessed only the surface of PA. The average specific capacitance values, C_{avg} (F g^{-1}) of the samples are estimated from the discharge process according to the following equation.[62, 63]

$$C_g = I\Delta t/\Delta V \times m \quad (1)$$

where I is the current loaded (A), Δt is the discharge time (s), ΔV is the potential change during discharge process, and m is the mass of the active material in a single electrode (g). The representative charge/discharge curves at a current density of 0.1 A g^{-1} are shown in Figure 7. Though, the CS/PANI exhibiting comparatively better performance than others, the stability of the PANI is not appreciable.[64] Thus, the composite CH-GO-ZnO/PANI has exhibiting superior performance in terms of stability.[65] It can be seen that the charge curves almost linear and

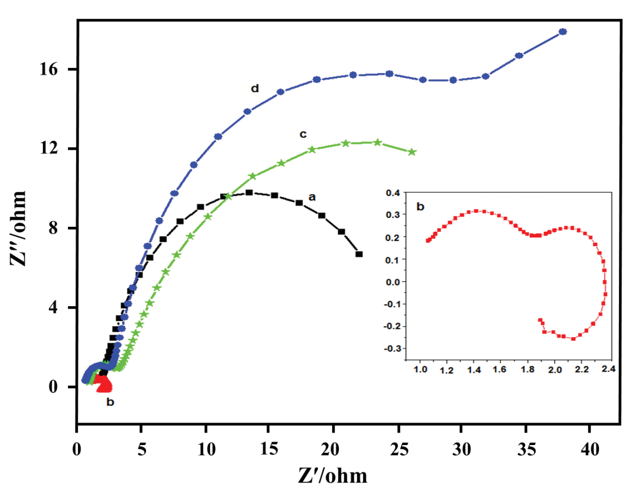

Figure 6. Nyquist impedance plot of hybrid composites (a) CS/PANI, (b) CS-GO/PANI, (c) CS-GO-ZnO/PANI and (d) CH-GO-ZnO/PANI (Inset figure shows lower scale value of CS-GO/PA hybrid composites).

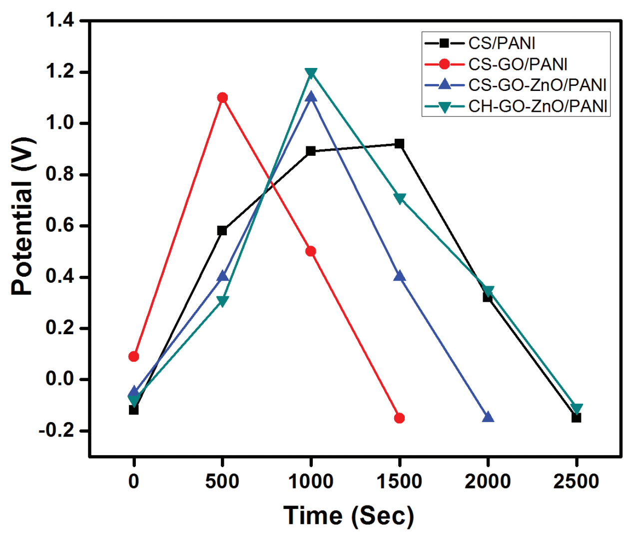

Figure 7. Galvanostatic charge/discharge cycling curves of different hybrid composites (a) CS/PANI, (b) CS-GO/PANI, (c) CS-GO-ZnO/PANI and (d) CH-GO-ZnO/PANI at a current density 0.1 A/g.

symmetrical to their discharge counterparts, indicating good electrochemical performance of the CH-GO-ZnO/PANI hybrid composites.

4. CONCLUSIONS

A simple and effective hybrid composite of chitin-base GO-ZnO/PANI were synthesized in a single bath. The functional group analysis was performed by FTIR and Raman scattering studies. The optical properties of prepared hybrid composites were studied using UV-Vis spectroscopy studies and results were discussed in detail. Surface morphological studies revealed the grains size variation in the prepared hybrid composites. CH-GO-ZnO/PANI hybrid composites exhibited the maximum value of specific capacitance of ∼542.63 F g^{-1}. The electrodes made of CH-GO-ZnO/PANI at 0.1 A g^{-1} current density could offered excellent specific capacitance and good rate capability. In future, CH-GO-ZnO/PANI composites will be given a dominant role as an electrode-active material for the high-performance supercapacitors application.

Acknowledgment: This research was supported by national nuclear R&D program through the National Research Foundation of Korea (NRF) grant (NRF-2015M2B2A4030705 and NRF-2015M2B2A9033138), the Ministry of Trade, Industry and Energy (MOTIE, 10051565) and Korea Display Research Corporation (KDRC) support program for the development of future devices technology for display industry.

References and Notes

1. K. Zhang, L. L. Zhang, X. S. Zhao, and J. Wu, *Chem. Mater.* 22, 1392 (**2010**).
2. M. M. Shaijumon, F. S. Ou, L. Ci, and P. M. Ajayan, *Chem. Comm.* 20, 2373 (**2008**).
3. L. Hu, J. W. Choi, Y. Yang, S. Jeong, F. L. Mantia, L. F. Cui, and Y. Cui, *PNAS* 106, 21490 (**2009**).
4. J. H. Sung, S. J. Kim, and S. H. Jeong, *J. Power Sources.* 162, 1467 (**2006**).
5. H. Zhu, X. Wang, F. Yang, and X. Yang, *Adv. Mater.* 23, 2745 (**2011**).
6. Y. Yang, D. Kim, M. Yang, and P. Schmuki, *Chem. Commun.* 47, 7746 (**2011**).
7. L. Huang, G. Guo, Y. Liu, Q. Chang, and Y. Xie, *J. Disp. Technol.* 8, 373 (**2012**).
8. J. T. Zhang, J. W. Jiang, H. L. Li, and X. S. Zhao, *Energy. Environ. Sci.* 8, 4009 (**2011**).
9. M. F. El-Kady, V. Strong, S. Dubin, and R. B. Kaner, *Science* 8, 1326 (**2012**).
10. C. Liu, F. Li, L. P. Ma, and H. M. Cheng, *Adv. Mater.* 8, E28 (**2010**).
11. T. Christen and M. W. Carlen, *J. Power Sources* 8, 210 (**2000**).
12. L. B. Hu, J. W. Choi, Y. Yang, S. Jeong, F. La Mantia, L. F. Cui, and Y. Cui, *Proc. Natl. Acad. Sci. USA* 8, 21490 (**2009**).
13. H. M. Zheng, T. Zhai, M. H. Yu, S. L. Xie, C. L. Liang, W. X. Zhao, S. C. Wang, Z. S. Zhang, and X. H. Lu, *J. Mater. Chem. C* 8, 225 (**2013**).
14. Y. Z. Liu, Y. F. Li, Y. G. Yang, Y. F. Wen, and M. Z. Wang, *Scripta Materials* 8, 301 (**2013**).
15. X. H. Lu, G. M. Wang, T. Zhai, M. H. Yu, J. Y. Gan, Y. X. Tong, and Y. Li, *Nano Lett.* 8, 1690 (**2012**).
16. F. H. Meng and Y. Ding, *Adv. Mater.* 8, 4098 (**2011**).
17. B. G. Choi, S. J. Chang, H. W. Kang, C. P. Park, H. J. Kim, W. H. Hong, S. Lee, and Y. S. Huh, *Nanoscale* 8, 4983 (**2012**).
18. H. J. Yu, J. H. Wu, L. Q. Fan, Y. Z. Lin, K. Q. Xu, Z. Y. Tang, C. X. Cheng, S. Tang, J. M. Lin, M. L. Huang, and Z. Lan, *J. Power Sources* 8, 402 (**2012**).
19. C. Z. Yao, B. H. Wei, L. X. Meng, H. Li, Q. J. Gong, H. Sun, H. X. Ma, and X. H. Hu, *J. Power Sources* 8, 222 (**2012**).
20. T. Lu, Y. Zhang, H. Li, L. Pan, Y. Li, and Z. Sun, *Electrochim. Acta* 8, 4170 (**2010**).
21. D. S. Yuan, T. X. Zhou, S. L. Zhou, W. J. Zou, S. S. Mo, and N. N. Xia, *Electrochem. Commun.* 8, 242 (**2011**).
22. B. J. Lee, S. R. Sivakkumar, J. M. Ko, J. H. Kim, S. M. Jo, and D. Y. Kim, *J. Power Sources* 168, 546 (**2007**).
23. G. Arabale, D. Wagh, M. Kulkarni, I. S. Mulla, S. P. Vernekar, K. Vijayamohanan, and A. M. Rao, *Chem. Phys. Lett.* 376, 207 (**2003**).
24. Y. Z. Zheng, M. L. Zhang, and P. Gao, *Mater. Res. Bull.* 42, 1740 (**2007**).
25. T. P. Gujar, V. R. Shinde, C. D. Lokhande, and S. H. Han, *J. Power Sources* 161, 1479 (**2006**).
26. G. M. Wang, H. Y. Wang, Y. C. Ling, Y. C. Tang, X. Y. Yang, R. C. Fitzmorris, C. C. Wang, J. Z. Zhang, and Y. Li, *Nano Lett.* 8, 3026 (**2011**).
27. J. Yan, E. Khoo, A. Sumboja, and P. S. Lee, *ACS Nano* 8, 4247 (**2010**).
28. S. M. Dong, X. Chen, L. Gu, X. H. Zhou, L. F. Li, Z. H. Liu, P. X. Han, H. X. Xu, J. H. Yao, H. B. Wang, X. Y. Zhang, C. Q. Shang, G. L. Cui, and L. Q. Chen, *Energy Environ. Sci.* 8, 3502 (**2011**).
29. T. Lu, L. K. Pan, H. B. Li, G. Zhu, T. Lv, X. J. Liu, Z. Sun, T. Chen, and H. C. D. Chua, *J. Alloys Compd.* 509, 5488 (**2011**).
30. S. Chen, J. Zhu, X. Wu, Q. Han, and X. Wang, *ACS Nano* 4, 2822 (**2010**).
31. Y. Zhang, H. Li, L. Pan, T. Lu, and Z. Sun, *J. Electroanal. Chem.* 634, 68 (**2009**).
32. G. Guo, L. Huang, Q. Chang, L. Ji, Y. Liu, Y. Xie, W. Shi, and N. Jia, *Appl. Phys. Lett.* 99, 83111 (**2011**).
33. Z. Li, Z. Zhou, G. Yun, K. Shi, X. Lv, and B. Yang, *Nanoscale Res. Lett.* 8, 473 (**2013**).
34. T. Lu, Y. Zhang, H. Li, L. Pan, Y. Li, and Z. Sun, *Electrochim. Acta* 8, 4170 (**2010**).
35. A. K. Geim and K. S. Novoselov, *Nat. Mater.* 6, 183 (**2007**).
36. Y.-Z. Long, M.-M. Li, C. Gu, M. Wan, J.-L. Duvail, Z. Liu, and Z. Fan, *Prog. Polym. Sci.* 36, 1415 (**2011**).
37. L. Nyholm, G. Nyström, A. Mihranyan, and M. Strømme, *Adv. Mater.* 23, 3751 (**2011**).
38. E. M. Geniès, A. Boyle, M. Lapkowski, and C. Tsintavis, *Synth. Met.* 36, 139 (**1990**).
39. C. Dhand, M. Das, M. Datta, and B. D. Malhotra, *Biosen. Bioelectron.* 26, 2811 (**2011**).
40. G. A. Snook, P. Kao, and A. S. Best, *J. Power Sources* 196, 1 (**2011**).
41. V. Khomenko, E. Frackowiak, and F. Beguin, *Electrochim. Acta* 50, 2499 (**2005**).
42. Y. G. Wang, H. Q. Li, and Y. Y. Xia, *Adv. Mater.* 18, 2619 (**2006**).
43. V. Gupta and N. Miura, *Electrochim. Acta* 52, 1721 (**2006**).
44. A. S. Arico, P. Bruce, B. Scrosati, and J. M. Tarascon, *Nat. Mater.* 4, 366 (**2005**).
45. K. Kurita, *Prog. Polym. Sci.* 26, 1921 (**2001**).
46. S. Anandhavelu and S. Thambidurai, *Mater. Chem. Phys.* 131, 449 (**2011**).
47. W. S. Hummers and R. E. Offeman, *J. Am. Chem. Soc.* 80, 1339 (**1958**).

48. F. Liu, B. Qin, L. He, and R. Song, *Carbohydr. Polym.* 78, 146 (**2009**).
49. K.-W. Park and J. H. Jung, *J. Power Sources* 199, 379 (**2012**).
50. L. M. Malard, M. A. Pimenta, G. Dresselhaus, and M. S. Dresselhaus, *Phys. Rep.* 473, 51 (**2009**).
51. K. Kurita, *Prog. Polym. Sci.* 26, 1921 (**2001**).
52. H.-Q. Wang, Z.-S. Li, Y.-G. Huang, Q.-Y. Li, and X.-Y. Wang, *J. Mater. Chem.* 20, 3883 (**2010**).
53. A. G. Yavuz and A. Gok, *Synt. Met.* 157, 235 (**2007**).
54. J. L. Wu, S. Bai, X. P. Shen, and L. Jiang, *Appl. Surf. Sci.* 257, 747 (**2010**).
55. J. L. Wu, X. P. Shen, L. Jiang, K. Wang, and K. M. Chen, *Appl. Surf. Sci.* 256, 2826 (**2010**).
56. W. J. E. Beek, M. M. Wienk, and R. A. J. Janssen, *Adv. Funct. Mater.* 16, 1112 (**2006**).
57. W. J. E. Beek, L. H. Slooff, M. M. Wienk, J. M. Kroon, and R. A. J. Janssen, *Adv. Funct. Mater.* 15, 1703 (**2005**).
58. A. G. Yavuz, A. Uygun, and H. K. Can, *Carbohydr. Res.* 346, 2063 (**2011**).
59. J. Rouquerol, D. Avnir, C. W. Fair bridge, D. H. Everett, J. M. Haynes, N. Pernicone, J. D. F. Ramsay, K. S. W. Sing, and K. K. Unger, *Pure Appl. Chem.* 66, 1739 (**1994**).
60. Q.-Y. Li, H.-Q. Wang, Q.-F. Dai, J.-H. Yang, and Y.-L. Zhong, *Solid State Ionics* 179, 269 (**2008**).
61. S. Najjar, D. Talaga, Y. Coffinier, S. Szunerits, R. Boukherroub, L. Servant, M. Couzi, and S. Bonhommeau, *Chem. Phys. Lett.* 514, 128 (**2011**).
62. V. A. Fonoberov, K. A. Alim, and A. A. Balandin, *Phys. Rev. B* 73, 165317 (**2006**).
63. W. Sugimoto, H. Iwata, K. Yokoshima, Y. Murakami, and Y. Takasu, *J. Phys. Chem. B* 109, 7330 (**2005**).
64. L. Wang, Y. Ye, X. Lu, Z. Wen, Z. Li, H. Hou, and Y. Song, *Sci. Rep.* 3, 3568 (**2013**).
65. Q. Zhao, L. Ma, Q. Zhang, C. Wang, and X. Xu, *Journal of Nanomaterials* 2015, Article ID 850147, 15 pages (**2015**).

Received: 3 October 2015. Accepted: 18 January 2016.